Journal of Solid State Chemistry **143,** 77–85 (1999)
Article ID jssc.1998.8086, available online at http://www.idealibrary.com on IDEAL®

Hydrothermal Synthesis and Structures of Two Tetramethylammonium Iron Molybdates $(TMA)_2FeMo_6O_{20}$ and $[TMA]_2[Fe(H_2O)_6]Mo_8O_{26}$

J. Do, X. Wang, and A. J. Jacobson[1]

Department of Chemistry, University of Houston, Houston, Texas 77204-5641

Received March 12, 1998; in revised form November 4, 1998; accepted November 8, 1998

Two new compounds $(TMA)_2FeMo_6O_{20}$ and $[TMA]_2[Fe(H_2O)_6]Mo_8O_{26}$ have been synthesized by hydrothermal reactions. $(TMA)_2FeMo_6O_{20}$ crystallizes in the monoclinic space group $C2/m$; $a = 21.204(1)$ Å, $b = 7.6393(5)$ Å, $c = 8.4191(6)$ Å, $\beta = 104.602(1)^\circ$, $V = 1319.7(2)$ Å^3, $Z = 2$, ($R = 2.23\%$, $I > 2\sigma(I)$) $[TMA]_2[Fe(H_2O)_6]Mo_8O_{26}$ crystallizes in the space group $P2_1/n$; $a = 10.3945(5)$ Å, $b = 16.4103(8)$ Å, $c = 10.8935(5)$ Å, $\beta = 98.842(1)^\circ$, $V = 1836.1(2)$ Å^3, $Z = 2$ ($R = 2.07\%$ $I > 2\sigma(I)$). The structures of both compounds were determined by single crystal X-ray methods. The crystal structure of $(TMA)_2FeMo_6O_{20}$ consists of $^2_\infty[FeMo_6O_{20}]^{2-}$ layers separated by layers of tetramethylammonium cations. The $[FeMo_6O_{20}]^{2-}$ layers are built up by the interconnection of corner- and edge-sharing MoO_6 octahedral chains through FeO_6 octahedra. The arrangement of MoO_6 octahedra in the chains is identical to that found in the red potassium molybdenum bronze structure. In the $(TMA)_2FeMo_6O_{20}$ structure, the chains are connected into layers by bridging FeO_6 octahedra, in contrast to the bronze structure, where the chains are directly connected by sharing oxygen atoms. The structure of $[TMA]_2[Fe(H_2O)_6]Mo_8O_{26}$ is made up by packing of octahedral $[Fe(H_2O)_6^{2+}]$ cations and β-$[Mo_8O_{26}^{4-}]$ cluster anions. These building units are interconnected through hydrogen bonds. Tetramethylammonium cations provide charge balance.

INTRODUCTION

Iron molybdates are important components in catalysts for the selective oxidation of, for example, methanol to formaldehyde (1). Ferric molybdate, $Fe_2(MoO_3)_3$, is thought to be a key component but excess MoO_3 is also known to have a strong influence on the catalyst performance. Ferric molybdate catalysts are typically prepared by coprecipitation from aqueous solutions followed by calcination at 400–600°C (2). Pure ferric molybdate has previously been prepared by high-temperature hydrothermal synthesis (460°C) and by conventional solid state methods (3, 4). Iron molybdates containing Fe(II), for example, $Li_2Fe_2(MoO_4)_3$ (5), have also been described. We are currently investigating lower-temperature methods including hydrothermal synthesis for the preparation of mixed metal molybdenum-based oxide catalysts and catalyst precursors. Several new simple molybdenum oxides have recently been synthesized by using ammonium and alkylammonium cations as structure directing agents in hydrothermal reactions (6–9). Here we describe the synthesis and structures of two new molybdenum rich iron molybdates, $(TMA)_2FeMo_6O_{20}$ and $[TMA]_2[Fe(H_2O)_6]Mo_8O_{26}$, obtained hydrothermally by using tetramethylammonium as the counter cation.

EXPERIMENTAL

Preparation of $(TMA)_2FeMo_6O_{20}$

The reactants MoO_3 (0.0748g, 0.52 mmol), iron acetate(II) (0.0287g, 0.18 mmol), and $N(CH_3)_4OH \cdot 5H_2O$ (1.2188g, 9.3 mmol) were added to 3 ml (166 mmol) water and acidified with acetic acid. The initial pH was 3.20. The starting materials were placed in a 23-ml-capacity Teflon-lined stainless steel Parr hydrothermal bomb and heated at 180°C under autogenous pressure for 3 days. Afterward, the reactor was cooled to room temperature over a 1-day period (final pH = 3.14). The product was washed with water and dried in air. Dark blue plate crystals (~20% yield based on Mo) were obtained together with an unidentified second phase. The crystals are stable in air but dissolved slowly in water. Experiments over a wide range of reaction conditions, including reactant ratios, concentrations, pH, and cooling times, were made in an attempt to optimize the synthesis. Systematic changes in the initial pH (2.5–3.4) and reactant concentrations showed that the formation of this compound is very sensitive to the conditions. The compound is obtained only in the pH range of 2.7–3.3 and the mole ratio Mo/Fe > 3. Higher pH and a higher concentration of $TMAOH \cdot 5H_2O$ tend to lead to better crystals and

[1]To whom correspondence should be addressed.

0022-4596/99 $30.00

higher yields. We were unable to find reaction conditions that led to the formation of a single phase product.

Preparation of $[TMA]_2[Fe(H_2O)_6]Mo_8O_{26}$

The reactants MoO_3 (0.540g, 3.75 mmol), iron acetate(II) (0.2174g, 1.25 mmol), and $N(CH_3)_4OH \cdot 5H_2O$ (0.6550g, 5 mmol) were added to 5 ml (278 mmol) water and acidified with acetic acid. The initial pH was 3.18. The starting materials were placed in a 23-ml-capacity Teflon-lined stainless steel Parr hydrothermal bomb and heated at 180°C under autogenous pressure for 3 days and then cooled to room temperature over a 1-day period (final pH = 3.00). The product was washed with water. Transparent yellow polyhedral single crystals (~25% yield based on Mo) of $[TMA]_2[Fe(H_2O)_6]Mo_8O_{26}$ were recovered together with unidentified dark brown and black crystalline phases. The yellow crystals were air and water stable.

Characterization

The crystal structures of $(TMA)_2FeMo_6O_{20}$ and $[TMA]_2[Fe(H_2O)_6]Mo_8O_{26}$ were determined by single-crystal X-ray diffraction methods. Preliminary examination and data collection were performed on a SMART platform diffractometer equipped with 1K CCD area detector using graphite-monochromatized Mo$K\alpha$ radiation at room temperature. A hemisphere of data (1271 frames at 5 cm detector distance) was collected using a narrow-frame method with scan widths of 0.30° in ω and an exposure time of 30 s/frame. The first 50 frames were remeasured at the end of data collection to monitor instrument and crystal stability, and the maximum correction applied on the intensities was <1%. The data were integrated using the Siemens SAINT program (10), with the intensities corrected for Lorentz factor, polarization, air absorption, and absorption due to variation in the path length through the detector faceplate. The program SADABS was used for the absorption correction (11). Additional crystallographic details for $(TMA)_2FeMo_6O_{20}$ and $[TMA]_2[Fe(H_2O)_6]Mo_8O_{26}$ are described in Table 1. For $(TMA)_2FeMo_6O_{20}$, the observed Laue symmetry and the systematic extinction condition (hkl: $h + k = 2n + 1$) were indicative of the monoclinic space groups $C2/m$, $C2$, and Cm. The centrosymmetric space group $C2/m$ was assumed. A satisfactory refinement confirmed the correctness of this space group. Final cell constants were refined using 4607 reflections having $I > 10\sigma(I)$. For $[TMA]_2[Fe(H_2O)_6]Mo_8O_{26}$, the observed Laue symmetry and the systematic extinctions ($h0l: h + l = 2n + 1$ and $0k0: k = 2n + 1$) uniquely indicated the monoclinic space group $P2_1/n$. The final unit cell parameters and the orientation matrix were obtained from the least-square refinement using 3955 reflections having $I > 10\sigma(I)$.

TABLE 1
Crystallographic Data for $(TMA)_2FeMo_6O_{20}$ and $[TMA]_2[Fe(H_2O)_6]Mo_8O_{26}$

	$(TMA)_2FeMo_6O_{20}$	$[TMA]_2[Fe(H_2O)_6]Mo_8O_{26}$
Formula mass (amu)	1099.8	1495.87
Space group	$C2/m$ (No. 12)	$P2_1/n$ (No. 14)
a (Å)	21.204(1)	10.3945(5)
b (Å)	7.6393(5)	16.4103(8)
c (Å)	8.4191(6)	10.8935(5)
β (°)[a]	104.602(1)	98.842(1)
V (Å^3)	1319.7(2)	1836.1(2)
Z	2	2
T (K)	297(2)	298(2)
λ (Å)	0.71073	0.71073
μ (cm^{-1})	33.78	31.24
Absorption correction[b]	Empirical	Empirical
ρ (calc. g/cm^3)	2.768	2.705
Crystal size (mm^3)	$0.14 \times 0.14 \times 0.06$	$0.30 \times 0.10 \times 0.10$
2θ limits (°)	$5° \le 2\theta(MoK\alpha) \le 57°$	$5° \le 2\theta(MoK\alpha) \le 57°$
No. of all data	4211	10654
No. of variables	124	260
Goodness-of-fit	1.129	1.032
R[c]	0.0223	0.0207
R_w[d,e]	0.0581[d]	0.0528[e]
$(\Delta\rho)_{max}$; $(\Delta\rho)_{min}$ (e/Å^3)	0.896; −0.900	0.617; −0.530

[a] α and γ were constrained to be 90° in the refinement of cell constraints.
[b] The program SADABS (11) was used for the absorption correction.
[c] $R = \sum|F_o| - |F_c|/\sum|F_o|$ (based on reflections with $I > 2\sigma(I)$).
[d] $R_w = [\sum w(|F_o| - |F_c|)^2/\sum w|F_o|2]^{1/2}$; $w = 1/[\sigma^2(F_o^2) + (0.0347P)^2 + 0.58P]$; $P = [\mathrm{Max}(F_o^2, 0) + 2F_c^2]/3$ (all data).
[e] $R_w = [\sum w(|F_o| - |F_c|)^2/\sum w|F_o|2]^{1/2}$; $w = 1/[\sigma^2(F_o^2) + (0.0272P)^2 + 0.92P]$; $P = [\mathrm{Max}(F_o^2, 0) + 2F_c^2]/3$ (all data).

The initial positions for all atoms were obtained using direct methods and the structures were refined by full matrix least squares techniques with the SHELXTL crystallographic software package (12). For $(TMA)_2FeMo_6O_{20}$, the final cycle of refinement performed on F_o^2 with 1649 unique reflections afforded residuals $R_w = 0.0581$ and $R = 0.0223$ [based on $F_o^2 > 2\sigma(F_o^2)$]. All of the hydrogen atoms were found by a difference Fourier synthesis and refined isotropically. For $[TMA]_2[Fe(H_2O)_6]Mo_8O_{26}$, the final cycle of refinement performed on F_o^2 with 4219 unique reflections afforded residuals $R_w = 0.0528$ and $R = 0.0207$ [based on $F_o^2 > 2\sigma(F_o^2)$]. The TMA hydrogen atoms were included in calculated positions with isotropic displacement parameters. The water molecule hydrogen atoms were found by difference Fourier synthesis and refined isotropically. In both phases, no unusual trends were found in the goodness of fit as a function of F_o^2, $\sin\theta/\lambda$ and Miller indices. Final values of the atomic parameters and equivalent isotropic displacement parameters are given in Table 2.

The infrared spectra (KBr pellet method) were measured on a Galaxy FTIR 5000 series spectrometer (Fig. 1). For

TABLE 2
Atomic Coordinates ($\times 10^4$) and Equivalent Isotropic Displacement Parameters ($Å^2 \times 10^3$) for $(TMA)_2FeMo_6O_{20}$ and $[TMA]_2[Fe(H_2O)_6]Mo_8O_{26}$

	x	y	z	U_{eq}[a]
		$(TMA)_2FeMo_6O_{20}$		
Mo(1)	789(1)	0	4172(1)	12(1)
Mo(2)	574(1)	2610(1)	6989(1)	12(1)
Fe	0	0	0	17(1)
O(1)	1601(1)	0	5046(4)	23(1)
O(2)	349(1)	5000	6753(3)	18(1)
O(3)	517(1)	2342(2)	4414(2)	14(1)
O(4)	734(1)	0	2049(3)	19(1)
O(5)	1398(1)	2787(3)	7529(3)	24(1)
O(6)	487(1)	0	6406(3)	14(1)
O(7)	387(1)	2056(2)	8823(2)	19(1)
N	3285(2)	0	7589(5)	28(1)
C(1)	4008(2)	0	8367(7)	35(1)
C(2)	2992(3)	1604(8)	8096(7)	62(1)
C(3)	3185(3)	0	5774(7)	45(1)
		$[TMA]_2[Fe(H_2O)_6]Mo_8O_{26}$		
Mo(1)	777(1)	821(1)	899(1)	24(1)
Mo(2)	−243(1)	−695(1)	2360(1)	30(1)
Mo(3)	−2596(1)	360(1)	472(1)	28(1)
Mo(4)	−1582(1)	1906(1)	−1002(1)	33(1)
Fe	0	5000	0	32(1)
O(1)	2035(2)	951(1)	2058(2)	36(1)
O(2)	159(2)	1803(1)	568(2)	32(1)
O(3)	1701(2)	725(1)	−522(2)	26(1)
O(4)	−591(2)	450(1)	1804(2)	28(1)
O(5)	−913(2)	488(1)	−722(2)	26(1)
O(6)	−1510(2)	−863(1)	3148(2)	44(1)
O(7)	1055(2)	−494(1)	3480(2)	45(1)
O(8)	135(2)	−1767(1)	1901(2)	36(1)
O(9)	−3765(2)	158(1)	−748(2)	42(1)
O(10)	−3343(2)	286(1)	1749(2)	44(1)
O(11)	−2407(2)	1504(1)	336(2)	36(1)
O(12)	−1589(2)	2924(1)	−736(2)	50(1)
O(13)	−2816(2)	1737(2)	−2203(2)	48(1)
O(14)	1973(2)	5130(2)	−178(3)	50(1)
O(15)	−5329(3)	577(2)	3244(2)	48(1)
O(16)	−362(3)	6161(2)	−833(3)	56(1)
N	8913(2)	2391(2)	4157(2)	37(1)
C(1)	9032(6)	2991(4)	3204(6)	127(3)
C(2)	9128(8)	2824(4)	5346(5)	140(3)
C(3)	7668(6)	2020(4)	3989(11)	173(4)
C(4)	9970(4)	1764(2)	4196(4)	59(1)

[a] U_{eq} is defined as one-third of the trace of the orthogonalized U_{ij} tensor.

$(TMA)_2FeMo_6O_{20}$, the spectrum confirmed the presence of TMA ions in the structure, as evidenced by the bands observed at 3026 and 1481 cm^{-1}. Several bands in the region 947.1, 808.2, and 779.3 cm^{-1} arise from Mo–O stretching. The spectrum of $[TMA]_2[Fe(H_2O)_6]Mo_8O_{26}$ is very similar to that of $(TMA)_2FeMo_6O_{20}$ and shows characteristic TMA ions absorption bands (3034 and 1481 cm^{-1}), Mo–O bands (949.0, 920.1, 844.9, 709.8, and 633.6 cm^{-1}), and H_2O (3458 and 1620 cm^{-1}).

RESULTS

Structure of $(TMA)_2FeMo_6O_{20}$

Selected bond distances and angles for $(TMA)_2FeMo_6O_{20}$ are listed in Table 3. The structure of $(TMA)_2FeMo_6O_{20}$ is made up of $^2_\infty[FeMo_6O_{20}^{2-}]$ layers. The layers are separated by TMA^+ ions. The $[FeMo_6O_{20}^{2-}]$ layers are built up from two crystallographically distinct MoO_6 distorted octahedra and one unique FeO_6 octahedron. There are two different Fe–O distances, 2.011(3) Å (×2) and 2.128(2) Å (×4) (average 2.089 Å). A bond valence calculation (12) using the parameter for Fe(II)–O bonds gives a bond valence sum (BVS) value of 2.32 v.u. somewhat higher than expected for Fe^{II}. The MoO_6 octahedra are highly distorted with Mo–O bond lengths in the range 1.694(3)–2.626(3) Å (average 2.005 Å) for Mo(1) and 1.695(2)–2.327(2) Å (average 1.975 Å) for Mo(2). The nearest neighbor Mo–Mo distance is 3.2178(3) Å. The local coordination geometries of the $Mo(1)O_6$ and $Mo(2)O_6$ octahedra are shown in Fig. 2. Each MoO_6 octahedron has one short Mo=O bond (Mo(1)–O(1), 1.694(3) Å; Mo(2)–O(5), 1.695(2) Å). An additional short Mo–O distance is located in a *cis* position (Mo(1)–O(4), 1.762(3) Å; Mo(2)–O(7), 1.741(2) Å). Two bonds with much longer distances are *trans* to the short Mo–O distances. Two other Mo–O bonds are intermediate in length. The local coordination environment is typical for Mo(VI). The BVS (13) values calculated for Mo(1) and Mo(2) are 5.96 and 5.92, respectively, in good agreement with the expected value of 6.00 for Mo(VI). Six MoO_6 octahedral units combine together by sharing edges to form a $[Mo_6O_{22}^{8-}]$ unit (Fig. 2). These $Mo_6O_{22}^{8-}$ units are linked by sharing corner oxygen atoms (O2) to form an infinite linear chain of composition $[Mo_6O_{20}^{4-}]$ parallel to the *b* axis (Fig. 3). These chains are joined by sharing oxygen atoms (O4, O7) with FeO_6 octahedra to form layers. Each iron octahedron shares corners with six adjacent MoO_6 octahedra to give layers of composition $[FeMo_6O_{20}^{2-}]$ parallel to the *bc* plane, as shown in Fig. 3. The Fe–O bonds connecting infinite $[Mo_6O_{20}^{4-}]$ chains also give rise to elliptical holes in the layer with approximate dimensions 4.5 Å (between O(7) atoms in the [010] direction) by 6.0 Å (between O(2) atoms in the [001] direction). Identical layers are separated by a distance of $a/2$, but displaced relative to each other by a distance of $b/2$ along the [010] direction (Figs. 3 and 4). There are no interlayer bonding interactions except those between the anionic layers and the TMA^+ cations.

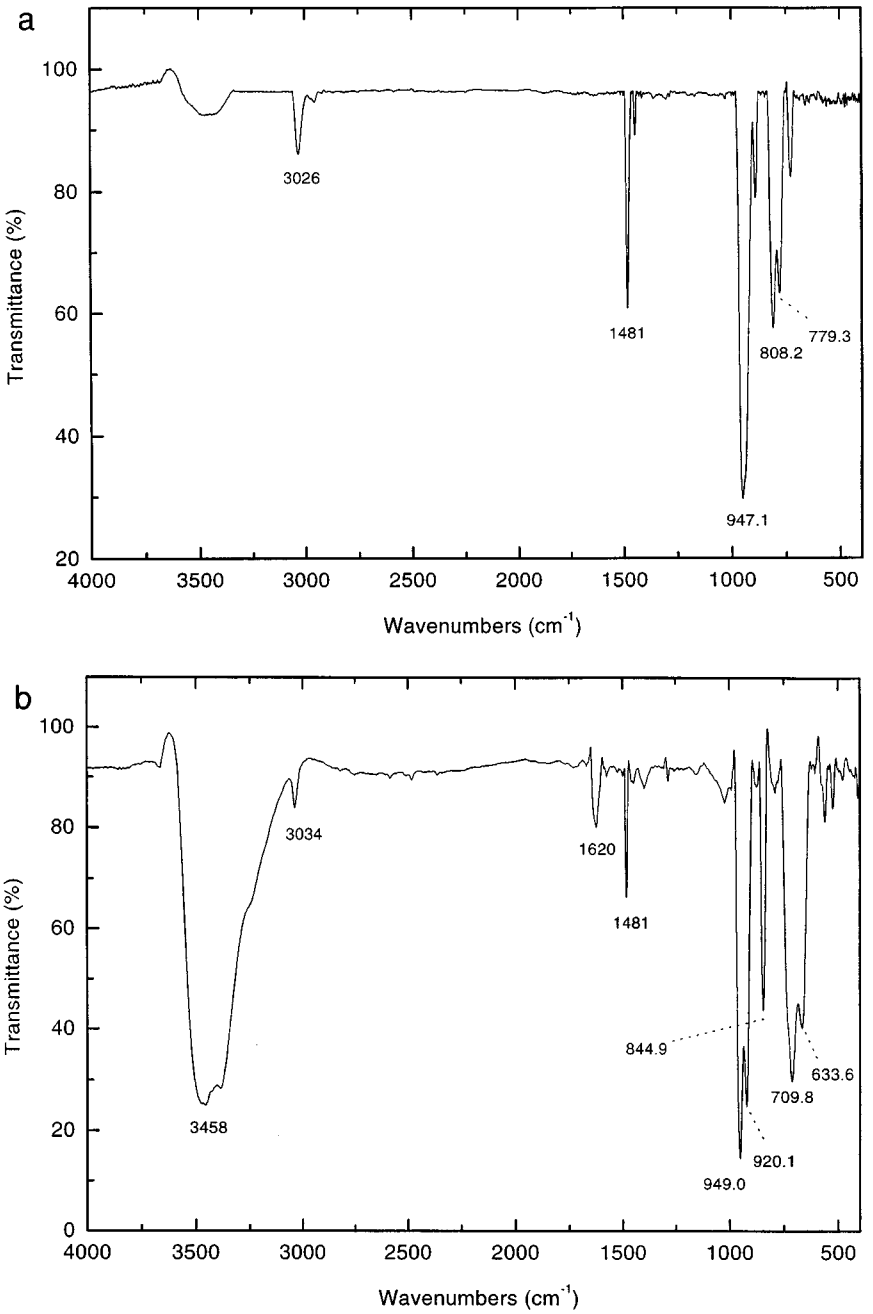

FIG. 1. Infrared spectra for (a) $(TMA)_2FeMo_6O_{20}$ and (b) $[TMA]_2\ [Fe(H_2O)_6]Mo_8O_{26}$.

Structure of $[TMA]_2[Fe(H_2O)_6]Mo_8O_{26}$

The structure of $[TMA]_2[Fe(H_2O)_6]Mo_8O_{26}$ is built up from TMA and octahedral $Fe(H_2O)_6$ cations and β-Mo_8O_{26} cluster anions (Fig. 5) (14). The iron atoms at the centers of the $Fe(H_2O)_6^{2+}$ octahedra are located on a special position between the molybdate ions. Between $Fe(H_2O)_6$, and β-Mo_8O_{26} groups there are hydrogen bonding interactions. The four TMA^+ cations per unit cell provide charge balancing. The arrangement of the $Fe(H_2O)_6$ and TMA cations and the β-Mo_8O_{26} anions in the unit cell is shown in Fig. 6. The $Fe(H_2O)_6$ units have a crystallographically imposed center of inversion and show approximate octahedral $m\bar{3}m$ molecular symmetry. The four crystallographically distinct MoO_6 groups in a β-Mo_8O_{26} cluster are highly distorted but adopt a typical two short, two intermediate, and

TABLE 3
Selected Bond Lengths (Å) and Angles (°) for $(TMA)_2FeMo_6O_{20}$

Mo(1)–O(1)	1.694(3)	Mo(2)–O(5)	1.695(2)
Mo(1)–O(4)	1.762(3)	Mo(2)–O(7)	1.741(2)
Mo(1)–O(3)#1	1.906(2)	Mo(2)–O(2)	1.8847(7)
Mo(1)–O(3)	1.906(2)	Mo(2)–O(6)	2.0508(6)
Mo(1)–O(6)	2.134(3)	Mo(2)–O(3)	2.150(2)
Mo(1)–O(6)#2	2.626(3)	Mo(2)–O(3)#3	2.327(2)
Mo(1)–Mo(2)	3.2178(3)		
Mo(1)–Mo(2)#1	3.2178(3)		
Fe–O(4)	2.011(3)	N–C(2)#1	1.485(5)
Fe–O(4)#4	2.011(3)	N–C(2)	1.485(5)
Fe–O(7)#5	2.128(2)	N–C(3)	1.489(6)
Fe–O(7)#6	2.128(2)	N–C(1)	1.508(6)
Fe–O(7)#3	2.128(2)		
Fe–O(7)#2	2.128(2)		
O(1)–Mo(1)–O(4)	103.9(1)	O(5)–Mo(2)–O(7)	103.4(1)
O(1)–Mo(1)–O(3)#1	104.81(6)	O(5)–Mo(2)–O(2)	99.6(1)
O(4)–Mo(1)–O(3)#1	99.44(7)	O(7)–Mo(2)–O(2)	102.8(1)
O(1)–Mo(1)–O(3)	104.81(6)	O(5)–Mo(2)–O(6)	99.6(1)
O(4)–Mo(1)–O(3)	99.44(6)	O(7)–Mo(2)–O(6)	87.1(1)
O(3)#1–Mo(1)–O(3)	139.6(1)	O(2)–Mo(2)–O(6)	155.7(1)
O(1)–Mo(1)–O(6)	96.6(1)	O(5)–Mo(2)–O(3)	94.03(9)
O(4)–Mo(1)–O(6)	159.4(1)	O(7)–Mo(2)–O(3)	154.62(8)
O(3)#1–Mo(1)–O(6)	74.91(6)	O(2)–Mo(2)–O(3)	92.15(9)
O(3)–Mo(1)–O(6)	74.91(6)	O(6)–Mo(2)–O(3)	71.77(8)
O(1)–Mo(1)–O(6)#2	165.5(1)	O(5)–Mo(2)–O(3)#3	165.58(9)
O(4)–Mo(1)–O(6)#2	90.6(1)	O(7)–Mo(2)–O(3)#3	90.50(8)
O(3)#1–Mo(1)–O(6)#2	72.20(6)	O(2)–Mo(2)–O(3)#3	80.73(9)
O(3)–Mo(1)–O(6)#2	72.20(6)	O(6)–Mo(2)–O(3)#3	76.99(8)
O(6)–Mo(1)–O(6)#2	68.8(1)	O(3)–Mo(2)–O(3)#3	71.56(9)
O(4)–Fe–O(4)#4	180.0	C(2)#1–N–C(2)	111.2(6)
O(4)–Fe–O(7)#5	95.36(7)	C(2)#1–N–C(1)	109.2(3)
O(4)#4–Fe–O(7)#5	84.64(7)	C(2)#1–N–C(3)	109.5(3)
O(4)–Fe–O(7)#6	95.36(7)	C(2)–N–C(1)	109.2(3)
O(4)#4–Fe–O(7)#6	84.64(7)	C(2)–N–C(3)	109.5(3)
O(7)#5–Fe–O(7)#6	95.1(1)	C(3)–N–C(1)	108.2(4)
O(7)#3–Fe–O(7)#2	95.1(1)		
O(4)#4–Fe–O(7)#3	95.36(7)		
O(4)–Fe–O(7)#3	84.64(7)		
O(7)#5–Fe–O(7)#3	180.0		
O(7)#6–Fe–O(7)#3	84.9(1)		
O(4)–Fe–O(7)#2	84.64(7)		
O(4)#4–Fe–O(7)#2	95.36(7)		
O(7)#5–Fe–O(7)#2	84.9(1)		
O(7)#6–Fe–O(7)#2	180.0		

Note. Symmetry transformations used to generate equivalent atoms: #1: $x, -y, z$. #2: $-x, -y, -z+1$. #3: $-x, y, -z+1$. #4: $-x, -y, -z$. #5: $x, -y, z-1$. #6: $x, y, z-1$.

two long Mo–O bond distance distribution within each MoO_6 octahedron (Fig. 5). The $Mo(1)O_6$ octahedron has one short Mo=O bond (Mo(1)–O(1), 1.686(2) Å), and an additional short Mo–O distance is located in a *cis* position (Mo(1)–O(2), 1.751(2) Å). The other MoO_6 octahedra have

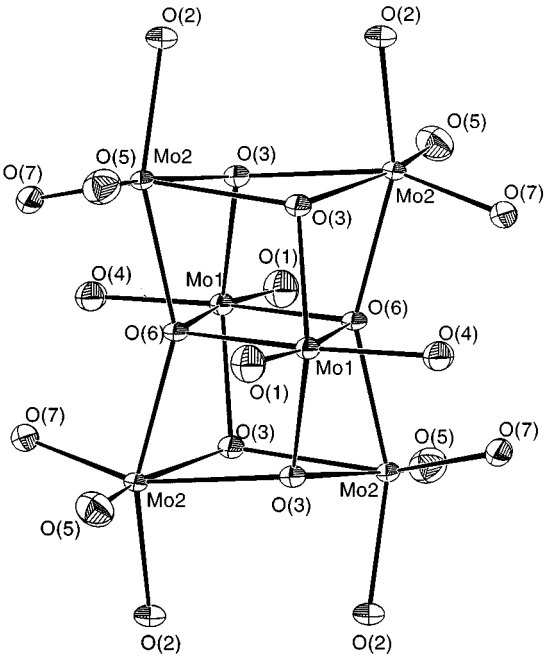

FIG. 2. Six MoO_6 units forming a hypothetical $(Mo_6O_{22})^{8-}$ polyanion. Compare Fig. 4 of Ref. (15).

similar geometries, each with two short Mo=O bonds in *cis* configurations. Each of the two short bonds is *trans* to a long Mo–O bond. All 12 hydrogen atoms in the $Fe(H_2O)_6$ octahedron make H bonds to nearby oxygen atoms of the β-Mo_8O_{26} clusters (Fig. 7). Each $Fe(H_2O)_6$ group is connected by hydrogen bonding interactions with six different neighboring β-Mo_8O_{26} clusters in an octahedral configuration (within O···O bond distance of 2.91 Å). Similarly, each β-Mo_8O_{26} cluster is linked to six $Fe(H_2O)_6$ groups in an octahedral configuration through hydrogen bonds. Three different types of H bonding interactions are observed in $[TMA]_2[Fe(H_2O)_6]Mo_8O_{26}$: [O(16)–H(5) ··· O(12)] in the [010] direction; [O(14)–H(6)···O(6); O(15)–H(3)···O(10)] in the $[10\bar{1}]$ direction; and [O(14)–H(1)···O(7); O(15)–H(2)···O(1); O(16)4–H(4)···O(13)] in the [101] direction. The BVS calculations for Mo(1), Mo(2), Mo(3), and Mo(4) yield values of 5.92, 5.98, 5.96, and 5.98 v.u., respectively, in reasonable accord with the 6.0 v.u. expected for Mo(VI). A bond valence sum value of 2.16 is calculated for the iron atom. The H bonding interactions between the $Fe(H_2O)_6$ and β-Mo_8O_{26} groups result in a pseudo-three dimensional structure. Selected bond distances and angles for $[TMA]_2[Fe(H_2O)_6]Mo_8O_{26}$ are given in Table 4.

DISCUSSION

The tetramethyl ammonium/molybdenum(VI)/iron(II)/oxygen system has been investigated by hydrothermal

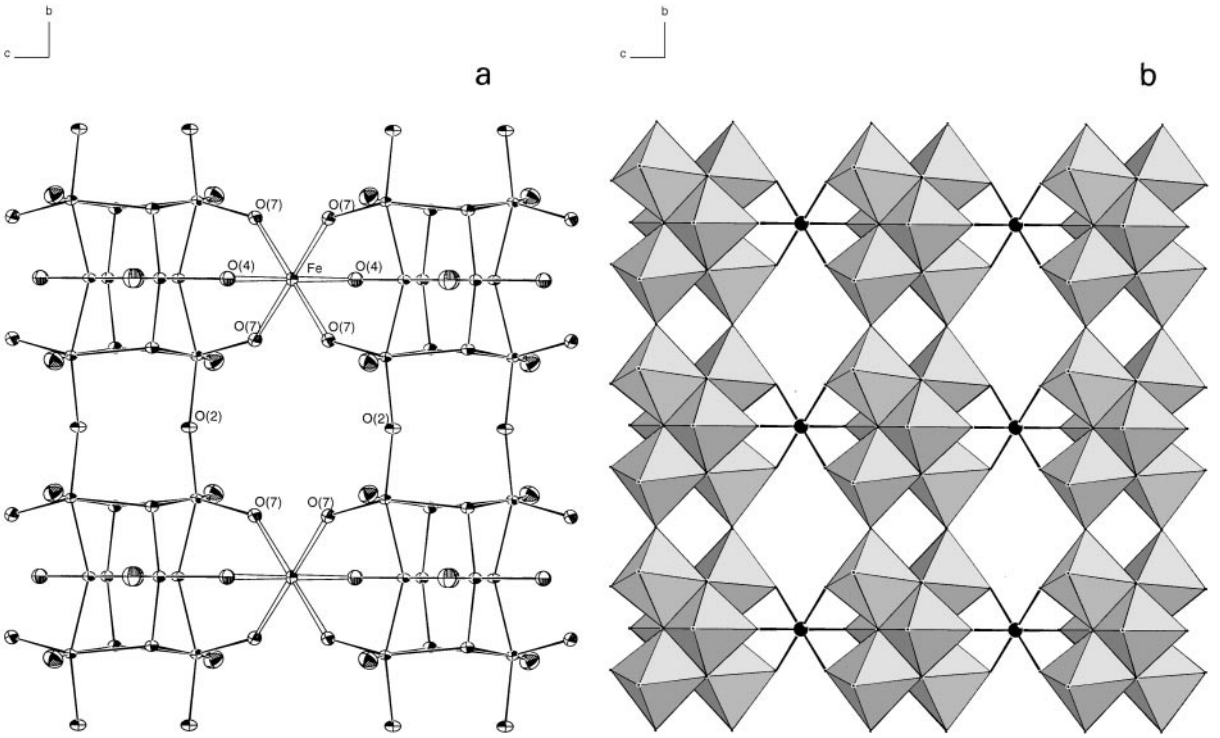

FIG. 3. $[FeMo_6O_{20}^{2-}]$ layer formed in $(TMA)_2FeMo_6O_{20}$ by connecting $[Mo_6O_{22}]^{8-}$ units and FeO_6 units. (a) View along *a* axis, showing the resulting six-rings and (b) polyhedral representation of one layer. The polyhedra represent the molybdenum octahedra and the filled circles are iron atoms.

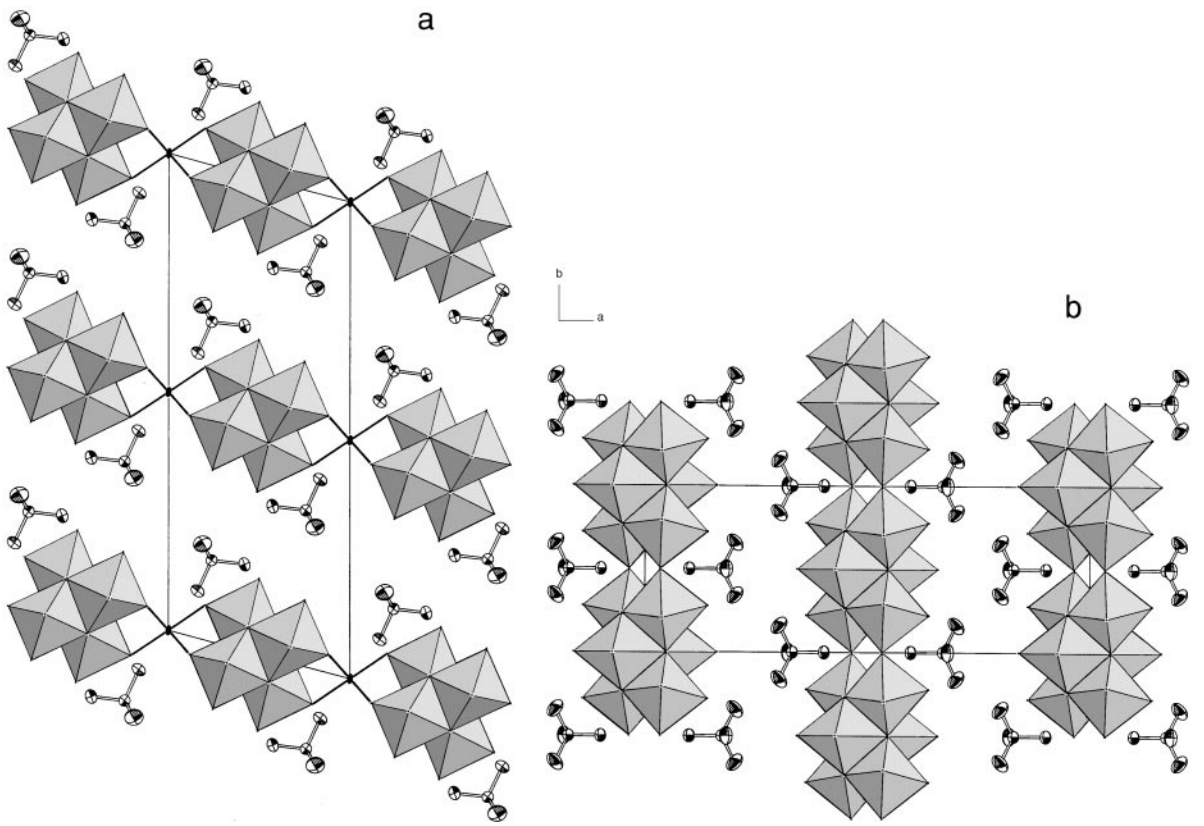

FIG. 4. Views of the $(TMA)_2FeMo_6O_{20}$ structure (a) parallel to [010] and (b) parallel to [001]. Thermal ellipsoids for the interlayer TMA^+ cations are shown with 50% probability.

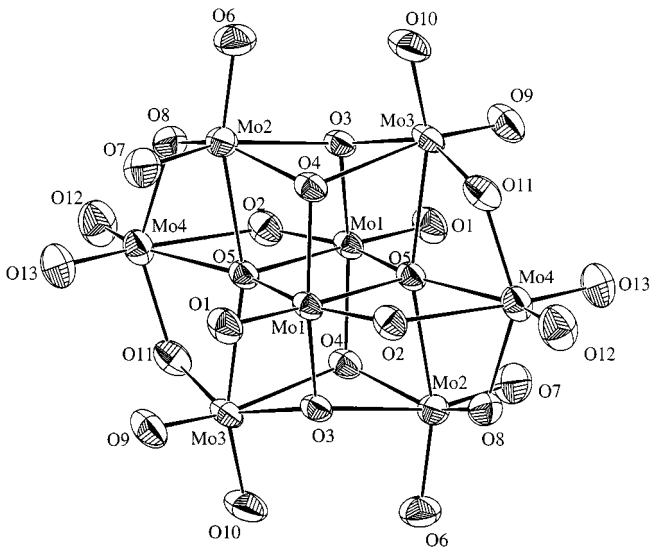

FIG. 5. The β-Mo_8O_{26} cluster in $[TMA]_2[Fe(H_2O)_6]Mo_8O_{26}$.

synthesis. Two new phases, $(TMA)_2FeMo_6O_{20}$ and $[TMA]_2[Fe(H_2O)_6]Mo_8O_{26}$, have been synthesized and structurally characterized by single-crystal X-ray diffraction techniques. In both structures, the coordination about the Fe atoms is only slightly distorted from ideal geometries, and the iron–oxygen distances are in good agreement with those calculated from crystal radii (15). The coordination environments of the Mo atoms are substantially distorted from a regular octahedron and are typical for Mo(VI). The structure of $[TMA]_2[Fe(H_2O)_6]Mo_8O_{26}$ contains isolated octamolybdate ions, whereas $(TMA)_2FeMo_6O_{20}$ has a layered structure containing molybdate chains linked by FeO_6 octahedra.

There is a structural relation between the $[Mo_6O_{22}]^{8-}$ anion in $(TMA)_2FeMo_6O_{20}$ and the $[Mo_8O_{26}]^{4-}$ unit in $[TMA]_2[Fe(H_2O)_6]Mo_8O_{26}$. If two Mo(4)–O(12),O(13) groups in the $[Mo_8O_{26}]^{4-}$ unit are taken away (Fig. 5), the $[Mo_6O_{22}]^{8-}$ unit is obtained (Fig. 2). The hydration of Fe^{2+} does not allow interconnection of the cluster anions in $[TMA]_2[Fe(H_2O)_6]Mo_8O_{26}$. The substantial difference in the syntheses of the compounds lies in the $TMAOH/H_2O$ ratio. For $(TMA)_2FeMo_6O_{20}$, $TMAOH/H_2O = 1/17.8$ and for $[TMA]_2[Fe(H_2O)_6]Mo_8O_{26}$, $TMAOH/H_2O = 1/55.6$, so hydration of Fe^{2+} in the latter is not unexpected.

The crystal structure of $(TMA)_2FeMo_6O_{20}$ is closely related to that of several molybdenum bronze phases such as red $K_{0.33}MoO_3$ (16), $(NH_4)_{0.33}MoO_3$ (17), blue $K_{0.28}MoO_3$(18), and $Cs_{0.25}MoO_3$ (19). In the red potassium and

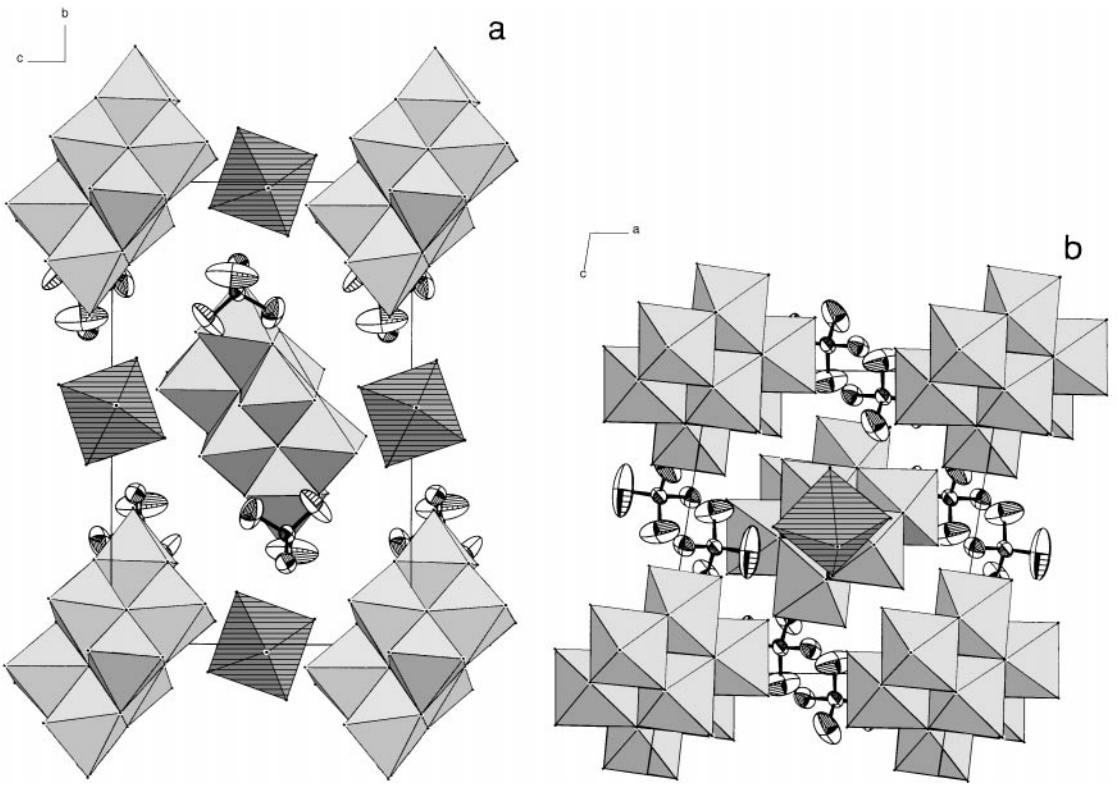

FIG. 6. Perspective views of the $[TMA]_2[Fe(H_2O)_6]Mo_8O_{26}$ structure along the (a) *a* axis and (b) *b* axis. The lighter and striped polyhedra represent the MoO_6 and $Fe(OH_2)_6$ octahedra, respectively. Thermal ellipsoids for the TMA cations are shown with 50% probability.

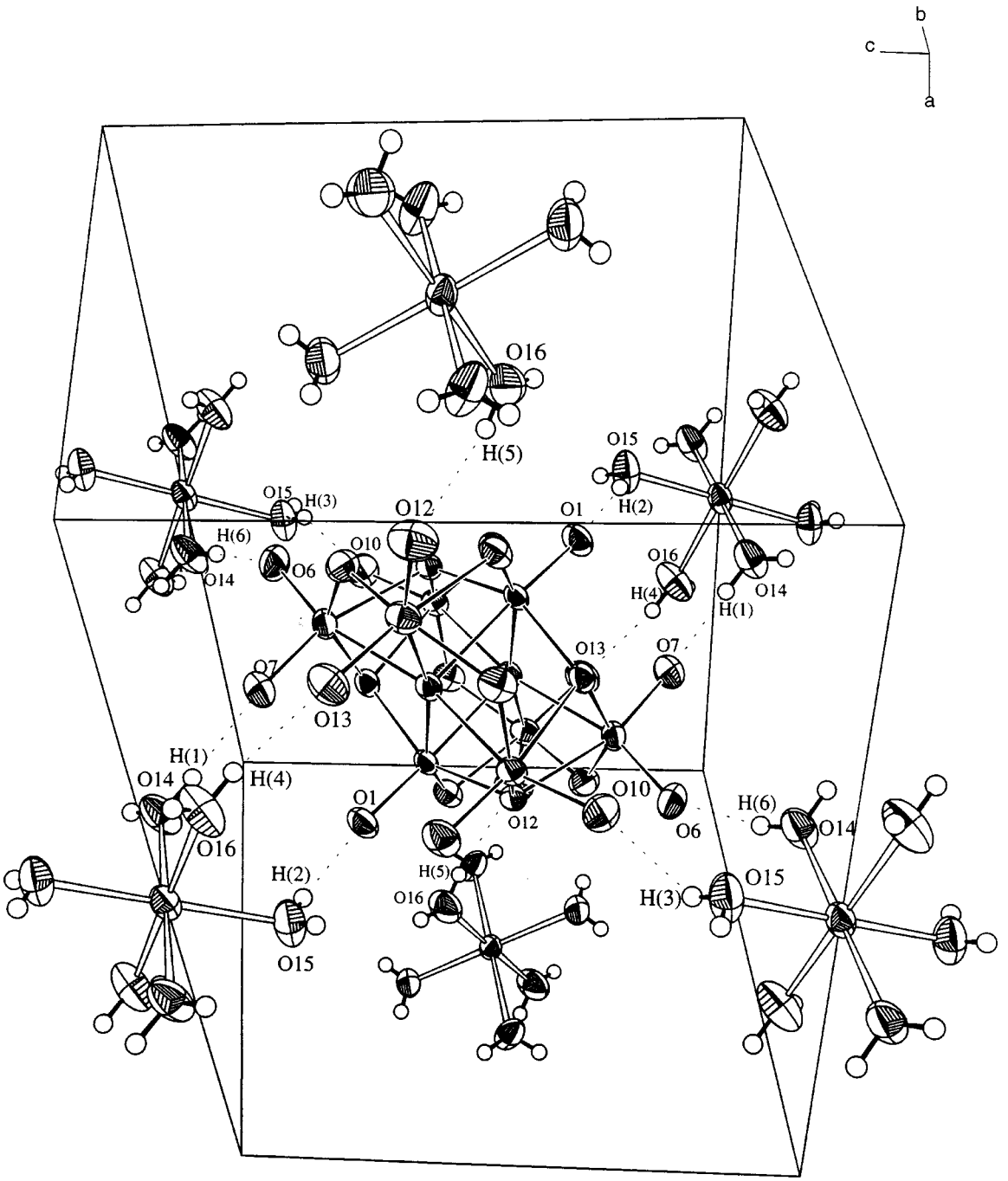

FIG. 7. View of the hydrogen bonding interactions between $Fe(H_2O)_6$ and β-Mo_8O_{26} units. TMA^+ cations are omitted for clarity.

ammonium molybdenum bronze phases, infinite linear $[Mo_6O_{20}^{4-}]$ chains are found. However, the $[Mo_6O_{20}^{4-}]$ chains are directly connected to each other by oxygen sharing to form an infinite layer of overall stoichiometry MoO_3. This layer is much denser than the $[FeMo_6O_{20}]^{2-}$ layer in $(TMA)_2FeMo_6O_{20}$ structure. In $(TMA)_2FeMo_6O_{20}$ the same infinite $[Mo_6O_{20}^{4-}]$ chains are linked by iron atoms to form the layer. In the red molybdenum bronzes, a fraction of the Mo^{6+} ions is reduced to provide charge compensation for the interlayer K^+ or NH_4^+ cations. In $(TMA)_2FeMo_6O_{20}$ the charge balance is achieved simply from the combination of Mo^{6+} and Fe^{2+} species. The dark blue color of the crystals and the calculated bond valence sums suggest the possibility of some charge transfer between the Mo and Fe. Further studies are in progress to investigate this more quantitatively.

TABLE 4
Selected Bond Lengths (Å) and Angles (°) for $[TMA]_2[Fe(H_2O)_6]Mo_8O_{26}$

Mo(1)–O(1)	1.686(2)	Mo(2)–O(6)	1.701(2)
Mo(1)–O(2)	1.751(2)	Mo(2)–O(7)	1.707(2)
Mo(1)–O(4)	1.949(2)	Mo(2)–O(8)	1.886(2)
Mo(1)–O(3)	1.949(2)	Mo(2)–O(4)	1.991(2)
Mo(1)–O(5)#1	2.163(2)	Mo(2)–O(3)#1	2.318(2)
Mo(1)–O(5)	2.356(2)	Mo(2)–O(5)#1	2.324(2)
Mo(3)–O(9)	1.690(2)	Mo(4)–O(12)	1.695(2)
Mo(3)–O(10)	1.698(2)	Mo(4)–O(13)	1.708(2)
Mo(3)–O(11)	1.897(2)	Mo(4)–O(11)	1.919(2)
Mo(3)–O(3)#1	2.005(2)	Mo(4)–O(8)#1	1.930(2)
Mo(3)–O(5)	2.344(2)	Mo(4)–O(2)	2.297(2)
Mo(3)–O(4)	2.354(2)	Mo(4)–O(5)	2.434(2)
Fe–O(14)	2.101(2)	N–C(3)	1.417(6)
Fe–O(14)#2	2.101(2)	N–C(1)	1.449(5)
Fe–O(15)#3	2.114(3)	N–C(2)	1.464(6)
Fe–O(15)#4	2.114(3)	N–C(4)	1.501(4)
Fe–O(16)	2.119(3)		
Fe–O(16)#2	2.119(3)		
O(14) ··· O(7)#1	2.740(3)		
O(14) ··· O(6)#2	2.853(3)		
O(15) ··· O(1)#3	2.909(4)		
O(15) ··· O(10)	2.859(4)		
O(16) ··· O(12)#4	2.867(4)		
O(16) ··· O(13)#5	2.795(4)		
O(1)–Mo(1)–O(2)	104.8(1)	O(6)–Mo(2)–O(7)	105.0(1)
O(1)–Mo(1)–O(4)	101.68(9)	O(6)–Mo(2)–O(8)	101.0(1)
O(2)–Mo(1)–O(4)	96.79(8)	O(7)–Mo(2)–O(8)	101.3(1)
O(1)–Mo(1)–O(3)	100.67(9)	O(6)–Mo(2)–O(4)	100.86(9)
O(2)–Mo(1)–O(3)	96.97(8)	O(7)–Mo(2)–O(4)	96.99(9)
O(4)–Mo(1)–O(3)	149.70(7)	O(8)–Mo(2)–O(4)	146.65(8)
O(1)–Mo(1)–O(5)#1	97.91(9)	O(6)–Mo(2)–O(3)#1	88.76(9)
O(2)–Mo(1)–O(5)#1	157.25(8)	O(7)–Mo(2)–O(3)#1	164.08(9)
O(4)–Mo(1)–O(5)#1	78.32(7)	O(8)–Mo(2)–O(3)#1	83.50(8)
O(3)–Mo(1)–O(5)#1	78.57(7)	O(4)–Mo(2)–O(3)#1	72.13(7)
O(1)–Mo(1)–O(5)	173.65(8)	O(6)–Mo(2)–O(5)#1	160.52(9)
O(2)–Mo(1)–O(5)	81.49(8)	O(7)–Mo(2)–O(5)#1	94.31(9)
O(4)–Mo(1)–O(5)	77.78(7)	O(8)–Mo(2)–O(5)#1	77.28(7)
O(3)–Mo(1)–O(5)	77.75(7)	O(4)–Mo(2)–O(5)#1	73.71(7)
O(5)#1–Mo(1)–O(5)	75.77(7)	O(3)#1–Mo(2)–O(5)#1	71.76(6)
O(9)–Mo(3)–O(10)	105.4(1)	O(12)–Mo(4)–O(13)	105.6(1)
O(9)–Mo(3)–O(11)	101.7(1)	O(12)–Mo(4)–O(11)	101.2(1)
O(10)–Mo(3)–O(11)	101.5(1)	O(13)–Mo(4)–O(11)	98.9(1)
O(9)–Mo(3)–O(3)#1	97.00(9)	O(12)–Mo(4)–O(8)#1	103.2(1)
O(10)–Mo(3)–O(3)#1	100.59(9)	O(13)–Mo(4)–O(8)#1	98.3(1)
O(11)–Mo(3)–O(3)#1	145.89(7)	O(11)–Mo(4)–O(8)#1	145.02(8)
O(9)–Mo(3)–O(5)	95.08(8)	O(12)–Mo(4)–O(2)	88.20(9)
O(10)–Mo(3)–O(5)	159.24(9)	O(13)–Mo(4)–O(2)	166.21(9)
O(11)–Mo(3)–O(5)	76.88(7)	O(11)–Mo(4)–O(2)	78.59(8)
O(3)#1–Mo(3)–O(5)	73.25(7)	O(8)#1–Mo(4)–O(2)	77.49(8)
O(9)–Mo(3)–O(4)	163.44(8)	O(12)–Mo(4)–O(5)	158.28(9)
O(10)–Mo(3)–O(4)	88.45(9)	O(13)–Mo(4)–O(5)	96.13(9)
O(11)–Mo(3)–O(4)	83.86(8)	O(11)–Mo(4)–O(5)	74.27(7)
O(3)#1–Mo(3)–O(4)	71.12(7)	O(8)#1–Mo(4)–O(5)	73.79(7)
O(5)–Mo(3)–O(4)	70.79(6)	O(2)–Mo(4)–O(5)	70.11(6)

TABLE 4—*Continued*

O(14)–Fe–O(14)#2	180.0	C(3)–N–C(1)	112.1(5)
O(14)–Fe–O(15)#3	89.2(1)	C(3)–N–C(2)	109.6(6)
O(14)#2–Fe–O(15)#3	90.8(1)	C(1)–N–C(2)	106.7(5)
O(14)–Fe–O(15)#4	90.8(1)	C(3)–N–C(4)	111.0(4)
O(14)#2–Fe–O(15)#4	89.2(1)	C(1)–N–C(4)	110.1(3)
O(15)#3–Fe–O(15)#4	180.0	C(2)–N–C(4)	107.2(3)
O(14)–Fe–O(16)	88.9(1)		
O(14)#2–Fe–O(16)	91.1(1)		
O(15)#3–Fe–O(16)	91.3(1)		
O(15)#4–Fe–O(16)	88.7(1)		
O(14)–Fe–O(16)#2	91.1(1)		
O(14)#2–Fe–O(16)#2	88.9(1)		
O(15)#3–Fe–O(16)#2	88.7(1)		
O(15)#4–Fe–O(16)#2	91.3(1)		
O(16)–Fe–O(16)#2	180.0		

Note. Symmetry transformations used to generate equivalent atoms: #1: $-x, -y, -z$. #2: $-x, -y+1, -z$. #3: $x+1/2, -y+1/2, z-1/2$. #4: $-x-1/2, y+1/2, -z+1/2$. #5: $-x-1/2, y-1/2, -z+1/2$.

ACKNOWLEDGMENTS

We thank the National Science Foundation (DMR9214804) and the R. A. Welch Foundation for financial support. This work made use of MRSEC/TCSUH Shared Experimental Facilities supported by the National Science Foundation under Award DMR9632667 and the Texas Center for Superconductivity at the University of Houston.

REFERENCES

1. B. C. Gates, J. R. Katzer, and G. C. A. Schuit, "Chemistry of Catalytic Processes." McGraw-Hill, New York, 1979.
2. H. Zhang, J. Shen, and X. Ge, *J. Solid State Chem.* **117,** 127 (1995).
3. H. Chen, *Mater. Res. Bull.* **14,** 1583 (1979).
4. W. T. A. Harrison, *Mater. Res. Bull.* **30,** 1325 (1995).
5. C. C. Torardi and E. Prince, *Mater. Res. Bull.* **21,** 719 (1986).
6. W. T. A. Harrison, L. L. Dussack, and A. J. Jacobson, *Inorg. Chem.* **33,** 6043 (1994).
7. M. I. Khan, Q. Chen, and J. Zubieta, *Inorg. Chim. Acta* **213,** 325 (1993).
8. Y. Xu, L.-H. An, and L.-L. Koh, *Chem. Mater.* **8,** 814 (1996).
9. R. C. Haushalter and L. A. Mundi, *Chem. Mater.* **4,** 31 (1992).
10. SAINT, Version 4.05. Siemens Analytical X-ray Instruments, Madison, WI, 1995.
11. G. M. Sheldrick, Program SADABS. University of Gottingen, 1995.
12. G. M. Sheldrick, SHELXTL, Version 5.03. Siemens Analytical X-ray Instruments, Madison, WI, 1995.
13. N. E. Brese and M. O'Keeffe, *Acta Crystallogr. Sect. B* **47,** 192 (1991).
14. W. G. Klemperer and W. Shum, *J. Am. Chem. Soc.* **98,** 8291 (1976).
15. R. D. Shannon, *Acta Crystallogr. Sect. A* **32,** 751 (1976).
16. N. C. Stephenson and A. D. Wadsley, *Acta Crystallogr.* **19,** 241 (1965).
17. K.-J. Range, K. Bauer, and U. Klement, *Acta Crystallogr. Sect. C* **46,** 2007 (1990).
18. J. Graham and A. D. Wadsley, *Acta Crystallogr.* **20,** 93 (1966).
19. W. G. Mumme and J. A. Watts, *J. Solid State Chem.* **2,** 16 (1970).